

ORBIT ERROR ESTIMATIONS FOR ESA'S COLLISION RISK PREDICTION SERVICE

H. Krag¹, H. Klinkrad¹, J. R. Alarcón-Rodríguez²

¹ESA/ESOC, Robert-Bosch-Str. 5, 64293 Darmstadt, Germany

²GMV, S.A., Isaac Newton 11, P.T.M. Tres Cantos, 28760 Madrid, Spain

OVERVIEW

As a result of the increasing number of space objects and the associated collision risk, collision avoidance processes are today important factors in space operations. ESA is monitoring close conjunctions of spacecraft with all other catalogued objects in a fully operational context. TLE data are used for all potential chaser objects. ESA's process, however, also allows to assess chaser orbits more accurately from tracking data generated within the last days before the event. All collision avoidance calculations make use of covariance matrices to characterise the uncertainty of the orbital position in space and time, considering errors in the orbit measurements, limitations of the TLE propagation method and uncertainties in the atmospheric drag. For the vast majority of space objects for which this information is not available, this data is reconstructed using residuals determined through a fit of numerically propagated orbits to the TLE datasets. The approach used for the estimation of TLE orbit covariances is explained in detail.

This paper outlines ESA's procedure for collision avoidance assessment and presents the techniques and principles applied in support of these. The different steps in the collision risk estimation process are explained from the detection of conjunctions, consideration of orbit uncertainties and their propagation and chaser orbit information refinement up to the avoidance manoeuvre planning. The concept will be illustrated by operational examples.

1. INTRODUCTION

1.1. The collision risk in LEO

The LEO altitude regime is the most frequently used region in space, and, today, the only region in which manned spacecraft are placed. As a consequence of this traffic, the global maximum of the spatial density of space objects is at around 800km altitude, where the influence of the atmosphere on the orbital lifetime is small. However, even in orbits used for human spaceflight (<450km altitude), despite of the denser atmosphere, the population of space objects is steadily evolving due to new fragmentations (approx. 5 per year) that over-compensate the decay of space objects.

Since the largest fraction of these objects are not detectable by the available sensors, space debris models, like ESA's MASTER (Meteoroid and Space Debris Terrestrial Environment) model are used to assess and describe the spatial distribution and physical properties of space objects in Earth orbits^[1]. FIG 1 provides a graphical representation of the distribution of orbital objects

according to MASTER-2005 for the two cut-off diameters 1cm and 10cm.

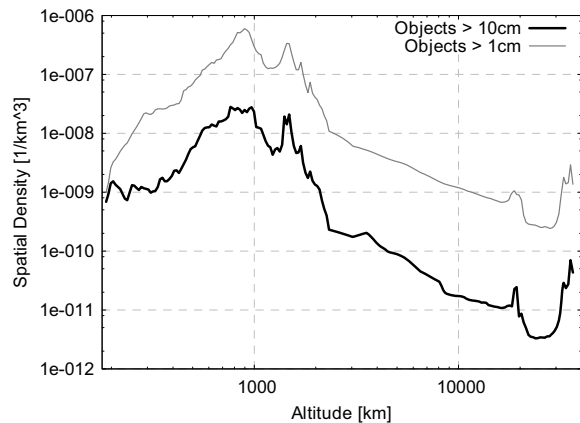


FIG 1. Spatial density of objects larger than 1cm and 10cm according to ESA's MASTER-2005 model

The parameter "spatial density" (number of objects per volume increment) is a suitable indicator for the distribution of the risk, since there is a linear relationship with the probability for an impact. The spatial density in LEO clearly prevails that in other altitudes for both diameter thresholds with a maximum at about 800km which again is about one magnitude above the average density in LEO. At relative velocities of up to 15km/s, LEO objects > 1cm can unfold sufficient energy to partly destroy spacecraft or penetrate the shields of the International Space Station (ISS) in case of collisions. MASTER predicts about 230,000 objects of that type residing in or crossing the LEO region. According to model predictions, a subset of approx. 12,000 of these objects is larger than 10cm. This diameter marks the theoretical performance limit of existing ground-based radar facilities for the tracking of objects in LEO. In fact, only about 7500 LEO objects can be found in the USSTRATCOM catalogue which is building up on regular measurements conducted by the US Space Surveillance Network. The remainder is believed to be missed out mainly due to geometric visibility constraints as a result of the attitude of the orbit plane and the short residence time in sensitive altitudes. Active collision avoidance is only possible for catalogued chaser objects, since it needs to rely on deterministic orbit information rather than on statistical flux data as provided by the ESA MASTER space debris model.

TAB 1 compares the mean times between collisions of space objects with a spherical target of 1m² cross-section for a few representative space missions. The numbers are a result of a collision flux analysis with MASTER-2005.

TAB 1. Mean time between collisions of objects with a spherical target of 1m² cross-section for some representative orbits

	d > 1 mm	d > 1 cm	d > 10 cm
ISS (360km)	1,480.38 y	191,791.33 y	3.03e+06 y
ERS (780km)	170.68 y	7,267.44 y	82,440.23 y
GStar (1,400km)	287.94 y	18,942.98 y	309,597.52 y
GPS (20,000km)	10,787.49 y	8.27e+06 y	1.41e+09 y
GEO (35,786km)	10,409.08 y	4.31e+06 y	6.00e+07 y

As expected from FIG 1 the impact risk is the highest in the ERS altitude. Collision avoidance processes in orbits above the LEO region seem not worthwhile for the current situation. One can also see that the mean time between collisions increases by more than an order of magnitude with each magnitude step in the cut-off diameter. Accordingly, the collision risk for the 10cm diameter threshold above which risk mitigation through collision avoidance is possible seems very low. However, collisions with such kind of objects are much more severe and in most cases leading to the complete loss of the mission and direct risk to human life in case of manned payloads.

The risk on operational payloads induced by these objects became evident through a total number of three detected collisions that all occurred in the past 15 years: The first confirmed, unintentional collision between two catalogue objects occurred on July 24, 1996, between the French Cerise satellite (95-033B), that was at the beginning of its operations at that time and a fragment (86-019RF) of an Ariane-1 H-10 upper stage which exploded about ten years before the event. In 2005, another two collision events could be identified a-posteriori from analysis of Space Surveillance data. In 1991, the abandoned Russian navigation satellite Cosmos 1934 collided with a fragment of a predecessor sister spacecraft COSMOS 926. In 2005, a 31-year-old US Thor Burner IIA final stage collided with an explosion fragment of a Chinese CZ-4B third stage.

These events underline that the risk for on-orbit collisions is a notable fact. In addition, it should be kept in mind that only collisions between catalogued objects are detectable from ground.

1.2. Risk reduction through collision avoidance

Using the figures of TAB 1 one can estimate the a priori risk for the loss of the ERS-2 mission (avg. cross-section approx. 109.4m² and mission duration ca. 12 years) due to a collision with an object larger than 10cm to be 1/63 and for the ISS (avg. cross-section approx. 1,500m² and 20 years mission duration) to be 1/101. For the largest (i.e. the catalogued) part of these objects, collision avoidance, and thus a significant risk reduction is possible. FIG 2 shows that a collision avoidance procedure can effectively reduce the risk due to these objects. The fractional residual risk (the risk that remains when evasive maneuvers are conducted compared to the risk when no maneuver is conducted) was computed for ERS-2 using ESA's DRAMA (Debris Risk Assessment and Mitigation Analysis) software^[2].

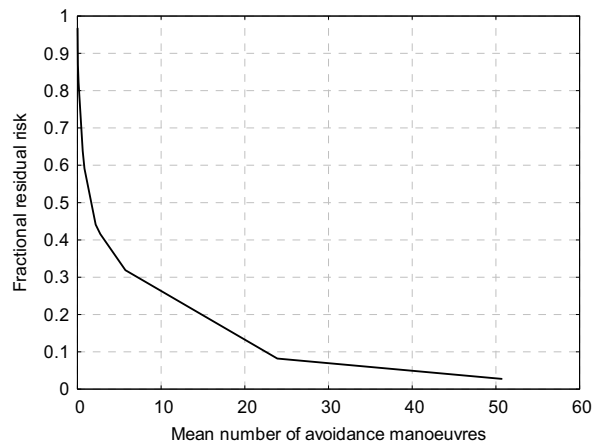


FIG 2. Risk reduction through collision avoidance maneuvers for ERS-2 (ESA's DRAMA S/W)

It should be noted that collisions should be avoided not only for the sake of protection of the own spacecraft but also to prevent the generation of new debris. Collision avoidance is thus a constant request of most of the existing debris mitigation guidelines in development and in use.

2. ESA'S COLLISION AVOIDANCE PROCESS

ESOC (the European Space Operations Centre) is providing collision avoidance services to ESA's major Earth observation mission since several years (ERS-1, ERS-2 and Envisat). The services and associated procedures in place are mission independent and could be applied to all kind of missions likewise. Different steps need to be performed in order to result in a decision for or against a collision avoidance manoeuvre. These steps, as explained in the following, are to a large degree implemented in the Collision Risk Assessment Software "CRASS"^[3].

2.1. Screening of conjunctions

The first step in a collision avoidance process is the determination of close conjunctions between the target and the space objects of the catalogue population. For the targets, ESOC uses orbit data generated from measurements by ESA's ground stations as used by the spacecraft operators. The only available data source for the chaser objects is the USSTRATCOM catalogue, which contains routinely updated orbit information in a so-called Two-Line Elements (TLE) format. This data is generated through tracking by on-ground radar and is coming with a simplified orbit representation (SGP4 – Simplified General Perturbations theory)^[4]. In ESA's approach, the most recent orbit information is collected every day through automatic download of TLEs and operational orbits. TLEs which have not been updated in the catalogue for an adjustable tolerance period are rejected. In the subsequent process, also scheduled daily, conjunctions are predicted over a timespan of 7 days. A numerical propagator is used for the prediction of target states and the SGP-4 orbit theory (the only applicable method) for the processing of TLE data. ESA's CRASS software uses a sieve algorithm to detect close conjunctions in the prediction interval. This algorithm employs two filter steps:

The first one is an altitude filter that rejects all risk objects whose orbits do not intersect the spherical altitude shell between the perigee and the apogee of the target orbit, taking the evolution of the orbits within the forecast interval into account. In a subsequent step, the relative range between target and chaser states is evaluated in a numerical process throughout the prediction interval. Chaser objects that are unable to penetrate a safety distance to the target in the analysed time frame are rejected. The safety distance is not applied unidirectionally, but follows the shape of an ellipsoid centered in the target with the largest dimension pointing into the along-track direction. In ESA's process, this ellipsoid extends 25km into the along-track (v) direction and both 10km into the radial (u) and out-of-plane (w) directions. Those objects that passed the two filter steps are forwarded to a root finding algorithm that searches the point of time in which the range rate between target and chaser is zero, i.e. the time of closest approach t_{tca} . FIG 3 demonstrates the performance of the different filter steps^[5]. An example for the misses that ERS-2 encounters per day is given in FIG 15. The number of encounters increases nearly linearly with the miss distance. The ellipsoidal control volume is typically intersected by about 10 objects per day. Only these close conjunctions are considered for the next processing step.

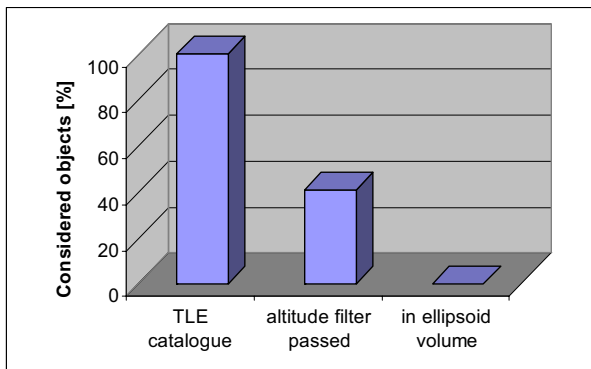


FIG 3. Effectiveness of the different conjunction event filter steps

2.2. Consideration of orbit uncertainties

Orbit determination products for both, the operational satellite of concern (hereafter referenced as target) and all potential chasers are input to the process. All orbit determination processes are based on the optimisation of orbit and object parameters along with an orbit prediction theory, to best match measurements of range, Doppler or directional angles. Due to the statistical nature of these processes along with the unavoidable measurement noise, all orbit information is associated with uncertainties. These are described by the so-called error covariance matrices that are generated during the orbit determination. The presence of these uncertainties also means that collisions between the target objects and chasers can not be identified in a deterministic manner, but conjunctions can only be evaluated together with the statistical risk for a collision based on orbit uncertainties. The decision for a collision avoidance maneuver is thus based on a threshold representing the maximum acceptable risk. In case of ESOC missions, this threshold risk is 1:2000 per conjunction event.

The operational orbit data that is used for the targets comes with accuracies on the order of 0.5m in radial, 1.0m in out-of-plane and 3.0m in along track direction. The accuracy of the TLE, used for the chasers, is about two orders of magnitude lower than that of the operational data. For both, targets and chasers, the covariance matrices are propagated to the relevant analysis epoch by means of transition matrices. An example for the result of the covariance propagation is given in FIG 4. This figure compares the evolution of the 1σ uncertainty for an operational and the corresponding TLE orbit in transversal (along track) direction, in which uncertainties are the largest in LEO.

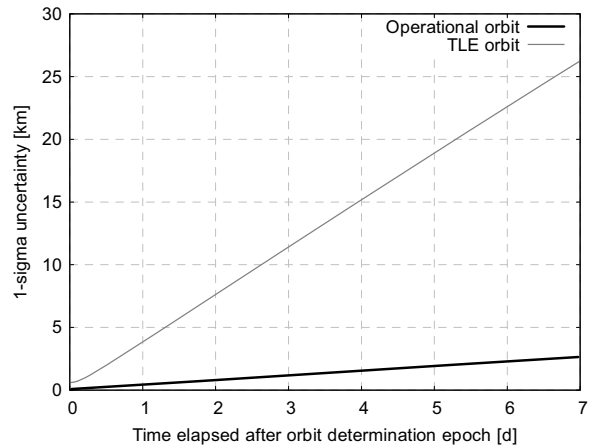


FIG 4. Evolution of 1σ uncertainties (TLE and operational data) in transversal direction for Envisat, epoch: April 26th, 2007

The example shows how significant the exact knowledge of the initial covariance is for the determination of the collision risk. However, a metric for the uncertainties connected with given TLE sets is not available to the general user. The necessary covariance information needs to be reconstructed with the use of the limited information coming with the TLE sets themselves. Since this is a common problem for all collision risk procedures running independently from USSTRATCOM data providers, different approaches for covariance estimation have been developed. ESA's approach will be presented in detail in section 3.

2.3. Determination of collision risk

The collision risk is determined for all close conjunctions that have been identified through the previously described process. ESA's collision risk assessment software makes use of formulations provided by Alfried and Akella^[6]. It is assumed that the position uncertainties of both, target and chaser, can be described by separate and uncorrelated Gaussian distributions. Further, the problem is simplified to a linear one, i.e. orbit curvatures and changes in the velocities are ignored.

After the propagation of the two error covariance matrices to the epoch of closest approach, they are combined into a common covariance matrix by simple addition of the two matrices. The 1σ position uncertainties expressed through the combined covariance span a three-dimensional error ellipsoid. In parallel, the combined target and chaser collision cross section is determined. Both objects are assumed to have a spherical cross section. A collision can

only occur if these two spheres intersect^[5]. This is the case when the stand-off distance is smaller than the sum of the radii of the two involved objects (with R_t and R_r being the radius of the target and risk object forming a combined collision cross section A_c with radius R_C according to Eq. 1).

$$(1) \quad R_C = R_t + R_r \quad A_C = \pi R_C^2$$

In order to simplify the computation of the probability for this case (i.e. the collision probability), this three-dimensional problem is reduced to a two-dimensional one through projection of the conjunction geometry and uncertainties onto the B-plane. The B-plane is perpendicular to the relative velocity Δv_{fca} at the time of conjunction and contains the conjunction range vector Δr_{fca} . The projection transforms the combined error ellipsoid into an ellipse and the spherical collision volume into circular collision area of the same radius. The problem is illustrated in FIG 5.

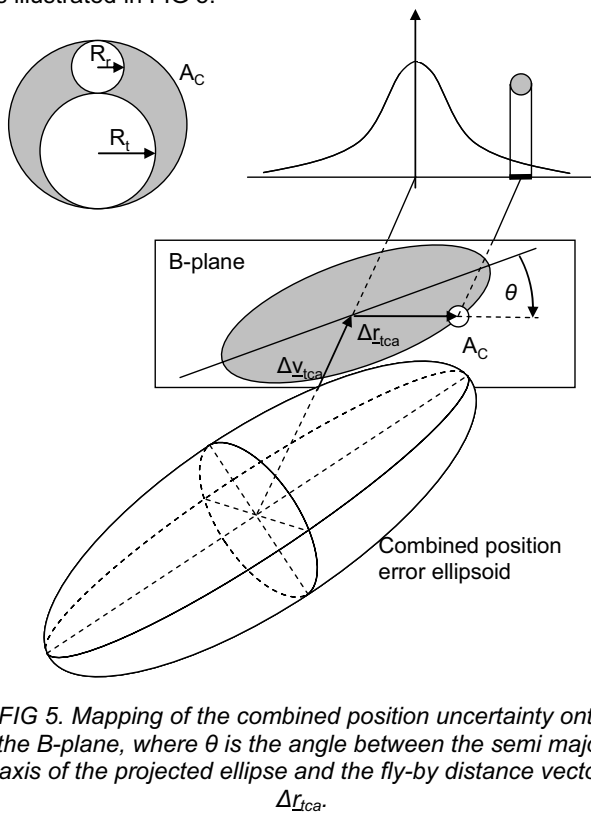


FIG 5. Mapping of the combined position uncertainty onto the B-plane, where θ is the angle between the semi major axis of the projected ellipse and the fly-by distance vector Δr_{fca} .

The two-dimensional Gaussian probability density for the combined position error in the B-plane is then integrated over the circular collision cross-section which is centered in the predicted fly-by location, separated by the stand-off distance from the maximum of the Gaussian, representing the most probable position error, centered at the target location^[5]. Information on the object radii and other object properties (cross section, type, name and identifiers) is taken from ESA's DISCOS database.

In ESA's process, only the ten highest risk conjunction events are presented to the operators. The collision risk assessment software automatically compiles a bulletin for these highest risk conjunction events and distributes it by Email. A warning label is attached when the mission-dependent risk threshold is violated by at least one conjunction event. The bulletin contains all relevant

information on the conjunction geometry and uncertainties in order to allow space debris analysts and mission operators to make a decision for or against a collision avoidance maneuver.

2.4. Avoidance maneuvers

Avoidance maneuvers require careful preparation, for which at least half a day needs to be accounted for. The decision for a manoeuvre is usually taken not earlier than 1 day before the conjunction event in order to take into account latest TLE sets for the chaser object and to allow for additional data to come in (e.g. tracking data, USSTRATCOM results). Determining the most efficient avoidance maneuver is a classical optimisation problem for the orientation of the delta-velocity vector in order to achieve a maximum flyby distance between the two objects with a minimum magnitude of the delta-velocity (Δv).

In practice, one can classify avoidance maneuvers into two groups (see FIG 6): In long-term maneuver strategies, a larger along-track separation of the objects is achieved through a slight change to the semi major axis some revolutions before the event. This introduces a shift for the time when the target is passing through the predicted encounter point. After the conjunction the original semi major axis is typically restored.

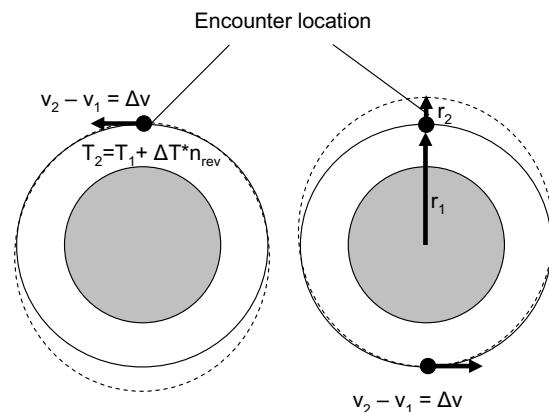


FIG 6. Long-term (left) and short-term (right) strategies for collision avoidance maneuvers^[2]

Some missions, e.g. Earth observation missions, have stringent requirements on the conservation of their ground-track repeat pattern, which is deteriorated through this first approach. In this case, the second manoeuvre strategy is preferred, which is executed on the short-term. An along track Δv is performed half a revolution before the conjunction, thus at the opposite point. This introduces both, a radial separation and an along-track separation at the encounter point. Another half revolution after the conjunction, the same Δv is given into the opposite direction, restoring the original orbit and recovering the ground track repeat pattern. This second class of maneuver, however, is less propellant efficient than the first type when similar miss distances are to be achieved.

Whenever an avoidance maneuver is planned, as part of this process the post maneuver trajectory is screened for new high-risk conjunction events resulting from the orbit change over the same timespan. In ESA's process, such a

screening is also applied prior to major orbit correction manoeuvres.

2.5. Improvement of chaser orbit information

Collision avoidance maneuvers, which are unplanned, have a direct impact on the mission lifetime and in some cases on the quality of the mission products. On the other hand the collision risk based decision threshold comes with a significant false alarm rate, i.e. most of the maneuvers conducted after the collision risk exceeded a threshold level have actually been unnecessary. This problem could be overcome when more accurate orbit information on the chaser objects is available. This can only be generated through dedicated tracking campaigns from ground followed by an orbit determination process under control of the risk analysts so that access to all necessary information and by-products is maintained.

For this purpose, ESOC is collaborating with the most prominent European radar tracking facilities^[5]: The TIRA instrument (Tracking and Imaging Radar), a 34m and 1MW peakpower monopulse radar operating in L-band, which is operated by FGAN (Research Establishment for Applied Sciences, near Bonn, Germany) and the two Armor radars (C-band, 10m dish and 1MW peakpower) located on the Monge tracking ship operated by the French Ministry of Defence. In case of high risk conjunctions and if visibility allows, such facilities are tasked with the tracking of at least three passages as close to the conjunction epoch as possible, starting typically one or two days before that epoch. Precise orbits and orbit covariances are obtained in the subsequent offline orbit determination process and are fed back into the collision risk estimation. Orbit uncertainties are typically reduced by more than an order of magnitude which again reduces the maneuver rate by a factor of about 20 for ESA's collision risk threshold of 1:2000. The dependency between the accepted collision probability and the mean number of maneuvers per year for both original (TLE) and refined orbit information (through dedicated tracking) is described by FIG 7.

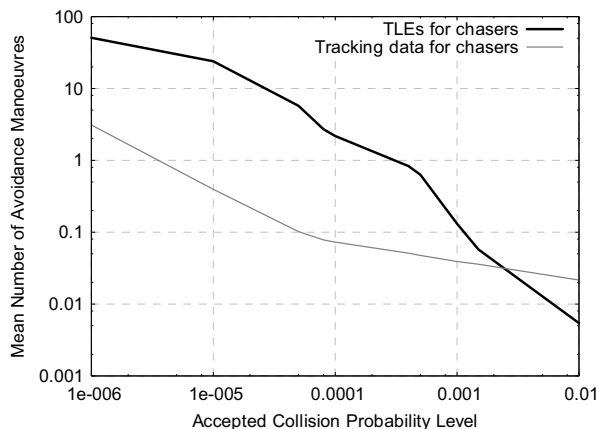


FIG 7. Reduction of the collision avoidance maneuver rate through improvement of chaser orbit information for ERS-2 (ESA's DRAMA S/W)

The curves intersect at higher accepted collision probability levels since for TLEs, the chaser location probability is distributed over a larger ellipsoidal volume, leading to the reduction of peak probabilities, so that the

collision risk is underestimated in these cases. This shows that the selection of the appropriate threshold probability is complex and always connected with the available error covariance information.

3. ORBIT UNCERTAINTY ESTIMATION

In this section a closer look at the methods to reconstruct the missing error covariance information for TLEs shall be taken.

3.1. Approach applied at ESA

ESA's approach consists of a comparison of the TLE orbit with an accurate numerical orbit resulting from a least-squares fit of the TLE orbit^{[1],[5]}. The residuals obtained in this manner indicate the order of magnitude of the intrinsic error of the SGP4/SDP4 theory for the selected orbit. The fit is performed 0.5 days forward and backward from the TLE epoch. The initial orbit state and the drag coefficient are estimated. The numerical orbit propagation considers the MSISE-90 atmosphere model, lunar and solar gravity, radiation pressure and the Earth gravity field up to degree and order 30. The TLE orbit is sampled in steps of 60s. Measurements are evenly weighted. The initial state is the TLE state at epoch attached with a priori variances of 1km for the position and 0.001km/s for the velocity components.

This approach is only applied to a subset of representative TLEs. The results are stored in a look-up table, together with information on the orbit categories. With the help of this table CRASS attaches the associated covariance information to any TLE set used in the process. This method has the advantage that no additional processing is required for the integration of new TLE sets.

Care must be taken for the selection of representative objects, the categories according to which the covariances are to be filed and the associated sampling rate. Therefore, it needs to be taken into account that TLE accuracy is dependent on the selection effects of the Space Surveillance Network. Optical telescopes track deep space beyond the 5000km range, while radars track below. There is a strong dependency between accuracy and the number of tracks per day. Furthermore, there is a range⁻⁴ degradation of sensitivity for radar systems. Finally, there is a North/South asymmetry in the sensor distribution, as most SSN tracking stations are located in the 20N to 50N latitude fringe. Therefore, the following orbital parameters seem useful to serve as look-up table categories:

- inclination (influences observability (number of tracks per day))
- perigee altitude (influences decay rate and range dependent observability)
- eccentricity (influences the decay rate and the range dependent observability)

In the following, this approach shall be demonstrated for the characterization of uncertainties of potential ISS chaser orbits: FIG 8 plots all catalogue objects with perigee altitudes between 0 and 450km. Obviously, orbit inclinations cluster around 7°, 28°, 52°, 65°, 82° and 98°. Hence, an inclination sampling using steps of 10°, 15°, 20°

and 30° starting at 0° preserves the characteristic clusters. Concerning eccentricity, clusters around eccentricities of 0, 0.5 and 0.7 can be identified. For this population of objects, no particular altitude dependency could be identified. FIG 8 also shows the distribution of the selected samples in the eccentricity/inclination parameter space, demonstrating the adequacy of the selection with respect to the overall population. A tabular overview on the resulting orbit uncertainty estimates for the sample objects are presented in TAB 2. It can be seen that a few orbit classes, and thus entries in the look-up table, remain empty.

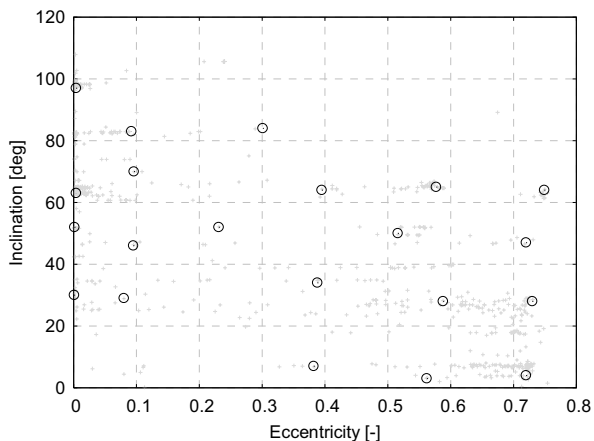


FIG 8. Distribution of selected sample objects (circles) (catalogue objects with perigees below 450km)

The results for the radial component are plotted in FIG 9 together with a least squares fit. Note that the error in the out-of-plane component has a different dependency on inclination than the errors in the other two components. It is interesting to observe that orbit uncertainties are generally the lowest at inclinations of 30°-60°. Since most SSN radar sensors reside in mid Northern latitudes, one might conclude that this constellation generates optimum observation conditions for these objects.

TAB 2. Orbit error estimates for the selected sample objects (perigees < 450km)

Inclination	Parameter	Eccentricity				
		<0.005	0.005 – 0.1	0.1 – 0.4	0.4 – 0.6	0.6 – 0.8
0°-20°	RAD (m)	-	-	1875	3079	5200
	A-T (m)	-	-	1540	3185	6131
	C-T (m)	-	-	508	333	1301
20°-40°	RAD (m)	119	458	940	2370	3845
	A-T (m)	349	816	807	2453	4263
	C-T (m)	149	276	2494	1809	2854
40°-60°	RAD (m)	109	127	110	459	1151
	A-T (m)	441	352	449	445	1300
	C-T (m)	202	918	1932	2471	3216
60°-80°	RAD (m)	132	216	603	415	1578
	A-T (m)	455	439	481	765	2046
	C-T (m)	163	515	2044	1522	3412
80°-100°	RAD (m)	118	227	932	-	-
	A-T (m)	626	436	956	-	-
	C-T (m)	155	196	490	-	-

Finally, the effect of the TLE date which produces different scenarios for the right ascension of ascending node and argument of perigee and thus different observation geometries has been analysed. TLEs of several epochs

have been used to analyse possible effects on the residuals and the correlation matrix. It was observed that the TLE epoch and the associated observation conditions combined with the different densities of the upper atmosphere do only have little influence on the residuals. The obtained values can thus be regarded as representative for each orbit.

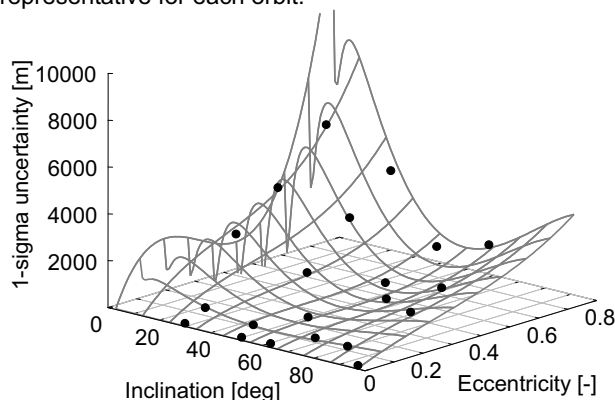


FIG 9. 1σ uncertainty in radial direction for the sample objects

3.2. Comparison with other approaches

One covariance estimation approach often applied makes use of pairs of TLE sets with subsequent orbit determination epochs. With the help of the SGP-4 theory, osculating states for both epochs and sets are generated and directly compared. TLE epochs match with the point of time at which the object passes through its ascending node. The deviation between the two states produced from each pair are assumed to describe the looked-for standard deviation, which can be split into the directional components of interest. Often, the results of several pairs are averaged to derive a standard deviation.

Objects, for which highly-accurate operational data is available a covariance estimate which is very close to the real one can be obtained through comparison of the operational data with the TLE prediction. For ERS-2 and Envisat such data is available. The resulting “real” covariance information for ERS-2 is compared to the estimates generated through the two methods in FIG 10, FIG 11 and FIG 12. For these figures, TLE orbits of all available epochs have been compared to the operational orbit in 1 minute steps and the resulting standard deviation is shown. Two very pronounced peaks can be identified in the curve representing the “real” covariance. The first peak, at around 45 days is resulting from an orbit correction maneuver while the second one at around 97 days is natural. The difference in the estimation quality between the two methods is remarkable. ESA’s approach using the residuals of a numerical fit seems to give better estimates in the absence of distortions. Due to the negligible time dependency identified above, fitted data is only presented for a small time frame and an average value is shown for all other epochs. This approach, however ignores the presence of large peaks (e.g. due to maneuvers) since only one TLE set is analysed at a time and single TLE sets are always self-consistent. The method can only identify the intrinsic error of the SGP4 theory, not the consistency of the transition from one set to the next.

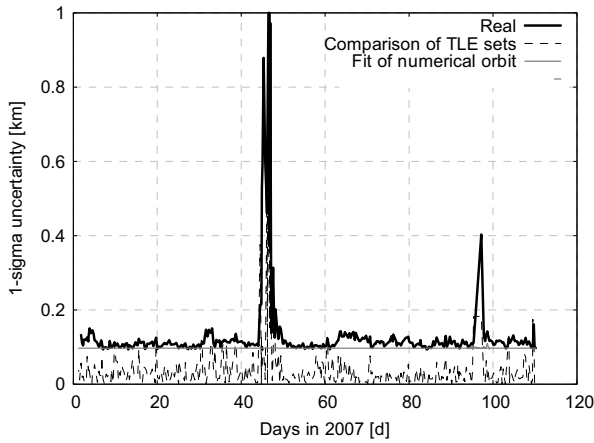


FIG 10. 1σ uncertainty of ERS-2 TLEs in radial direction determined by different methods

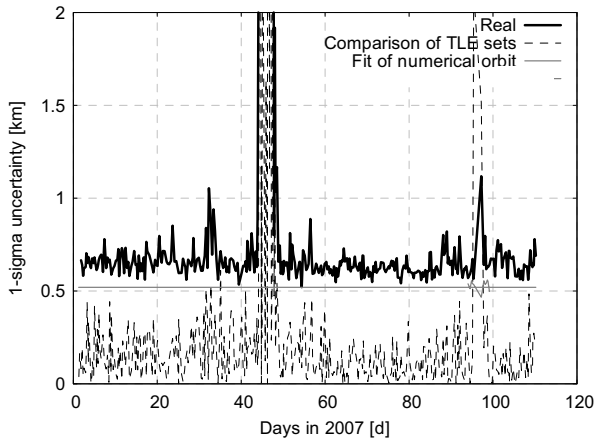


FIG 11. 1σ uncertainty of ERS-2 TLEs in along-track direction determined by different methods

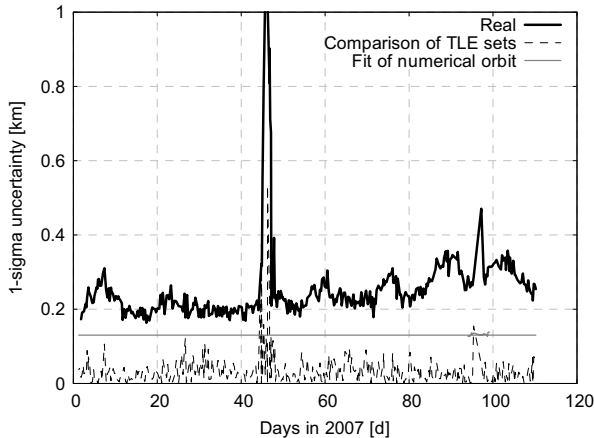


FIG 12. 1σ uncertainty of ERS-2 TLEs in out-of plane direction determined by different methods

The alternative method is somewhat complementary, however, it has to rely on the SGP4 theory, which reconstructs an osculating state from doubly averaged elements at a target epoch with the help of a simple analytical approach. The results are thus significantly diluted by orbit theory deficiencies. Also, TLE epochs are not uniformly distributed. Hence, the propagation error has a varying influence on the results. Finally, due to the fact that states at TLE epoch always are in the equatorial

plane, this method always encounters the same limitations of the SGP4 method w.r.t tesseral perturbations as a function of the longitude of the ascending node. In this example, the average error estimate is generally lower, while inconsistencies in the transition to new, distorted TLE sets are reflected in the results.

The remaining insufficiencies of the method applied by ESA are associated with reconstructed information on the drag coefficient, which is optimized to follow the trend of the simplified SGP4 long-term perturbation approach due to the fit. Another deficiency of the alternative method that compares pairs of TLE sets is that it relies on single values at one epoch rather than on averaged values. FIG 13 shows the deviation of the osculating states at each TLE epoch to the operational orbit (one per TLE set). On the average, these deviations meet the real figures, which represent the standard deviations between TLE and operational orbit computed over longer arcs. The large fluctuation shows that confidence in single values can only be very low.

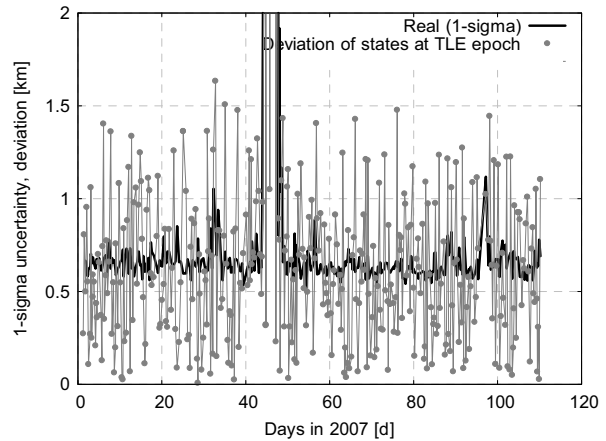


FIG 13. Offset of TLE states at epoch and mean deviation of TLEs (real 1σ) compared to the operational orbit

In general, the residuals obtained through a fit of an initial state and drag coefficient to a TLE set using a numerical propagator are good estimates for the uncertainties connected with the TLE orbits in particular for circular orbits in low altitudes. For higher eccentricities, the method applied here might, however, underestimate the position errors by an even larger degree. However, in view of the unavailability of the operational data for the chaser objects, the presented approach provides the best indication of the order of magnitude of the orbit errors.

4. RESULTS

4.1. Characterisation of predictions

In order to illustrate the characteristics of conjunction events, an overview on the results of ESA's CRASS software shall be presented. The statistics shown in the following have been generated from the ten highest risk daily conjunction predictions for the first quarter of 2007 for ERS-2 and Envisat. FIG 14 discriminates the conjunctions by object type. It is interesting to note that more than half of the encountered objects are intact (but not necessarily operational). Such object have large collision cross-

sections and are thus, despite of their smaller number, more frequent among the higher risk chasers.

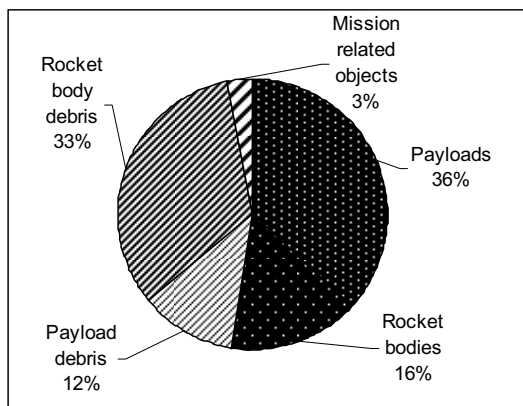


FIG 14. Statistics on the object types encountered by ERS-2 and Envisat in the first quarter of 2007

The minimum miss distance is an influencing factor for the collision risk (see FIG 15).

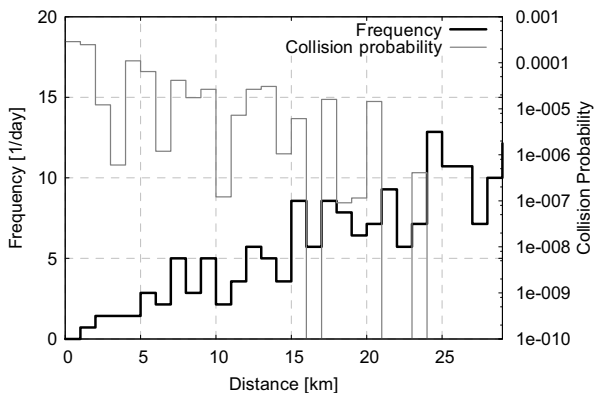


FIG 15. Histogram of encounter rate (left axis) and collision probability (right axis) as a function of the miss distance for ERS-2 and Envisat in the first quarter of 2007

However, close conjunctions only produce high collision risk when the angle θ between the semi major axis of the projected, combined error ellipse and the miss distance vector is small. The combined error covariance ellipsoid is dominated by the large uncertainties in the TLE chaser orbit. Hence, in LEO, the semi major axis will be close to the along-track direction of the chaser orbit. Collision probabilities are thus highest the closer the situation approaches an orthogonal conjunction geometry. The angle θ is often small when the approach occurs close to the horizontal plane, i.e. when the elevation angle under which the object is seen from the target is small. Accordingly, conjunction with low fly-by distances usually generate high collision risk in conjunction with low elevation angles. FIG 16 plots the elevation and minimum distance for different risk levels of the ERS-2 and Envisat flybys in the first quarter of 2007. This demonstrates that the miss distance alone is not a suitable criterion to decide on an avoidance maneuver.

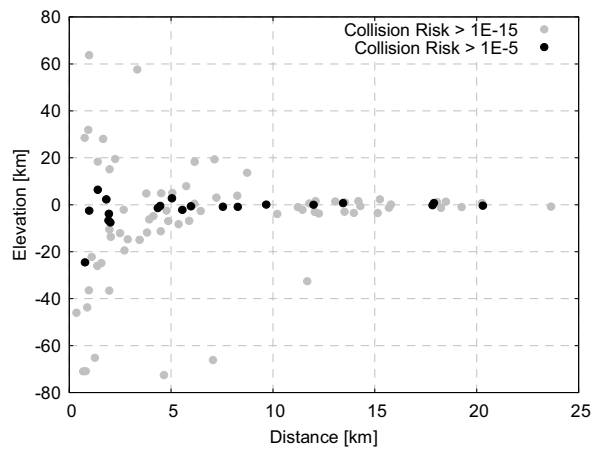


FIG 16. Elevation and miss distance of encounters for ERS-2 and Envisat in the first quarter of 2007

4.2. Operational examples

In the following ESA's collision avoidance service shall be demonstrated along with two operational examples from the year 2006.

The first example addresses a conjunction of Envisat with a COSMOS-3M second stage (COSMOS 1048 launched 1978) which was scheduled to occur on June 6th, 2006 at 11:38:09 UTC. Several days before, the automated collision risk assessment process raised a warning for this encounter. A collision probability of $1/1244$ and a miss distance of 252m one and a half day before the event.

COSMOS 1048 is a cylindrical object with a cross section of ca. 1.77m^2 and a mass of 743.31kg on a circular orbit with an inclination of 74° . The predicted conjunction geometry was close to orthogonal with an elevation angle of -13.75° and a relative velocity of 14.88km/s which is close to the theoretical average impact velocity for ERS-2 and Envisat. The FGAN Tracking and Imaging Radar produced six tracks of COSMOS 1048, for three successive passages on June 6th (with a maximum elevation of 83.1° and three successive passages on June 7th with a maximum elevation of 57.5°). The subsequent orbit determination process resulted in an orbit with 1σ uncertainties of only a few meters in radial and out of plane direction and only a few tens of meters in along track direction (compare with TAB 2 for uncertainty of corresponding TLE data). A repeated collision risk assessment generated a significantly reduced collision probability and a miss distance of 1072m, a number which was confirmed by US SSN experts using independent data (1149m). This generated sufficient confidence to decide that no evasive maneuver needed to be conducted.

Just some days later CRASS raised another warning for a conjunction event to occur between Envisat and a Scout G-1 4th stage (Altair IIIA, launched in 1983). The event was scheduled for June 20th, 2006 at 02:08:04 UTC. About 4 days before the event collision probability and miss distance were determined to be $1/2614$ and 180m and at the last prediction, 17h before they were $1/7179$ and 314m. The conjunction geometry was characterized through a high elevation of -72.19° and a relative velocity of 14.905km/s. The point of closest approach was determined to be at 796.5km altitude in high Northern

latitudes (78.93°) above the Pacific (longitude: 167.87°). The Scout G-1 rocket body is a comparably small object with a cross section of about 0.55m² and a mass of 23.7kg on a circular orbit with 82° inclination. While tracking with European facilities was not possible in this case, the conjunction was confirmed by SSN experts in the days before the event with a measured miss distance of 181m. The conjunction geometry is illustrated in FIG 17.

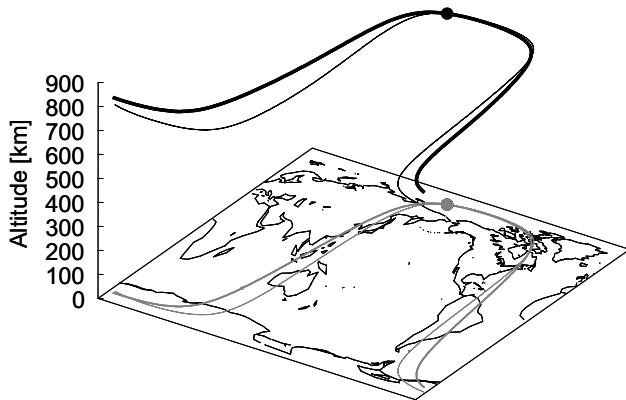


FIG 17: Conjunction geometry of Envisat (solid line) and a Scout G-1 rocket body (dotted line) one orbit around the conjunction epoch at June 20th, 2006

The good match between the predicted miss distances led to the decision to conduct an evasive maneuver. Half an orbit revolution before the event at 275° true latitude thrusters were commanded to generate a Δv of 40.0 mm/s in flight direction and, one revolution later, at the same position the same Δv was directed against the flight direction. This maneuver consumed approximately 300grams of hydrazine. Before the maneuver the modified Envisat orbit was screened for proper clearance. The corresponding risk prediction for this conjunction revealed a reduced collision probability of 1/23832 and a miss distance of 382m, which was considered acceptable.

5. CONCLUSIONS

ESA has developed an infrastructure for the screening of close conjunctions between USSTRATCOM catalogue objects and their LEO satellites. The underlying process from orbit data retrieval, determination of collision probability and event notification is fully automated. Independent European tracking data is used to generate accurate ephemerides and error covariances for the chaser objects to support any decision to maneuver. ESA's approach to derive error covariance information for TLEs consists of a comparison of a numerically propagated orbit fitted through a TLE with this TLE set. This approach has been found to reveal the characteristics of the uncertainties for all orbit classes and its results match more closely with the real covariance compared to other estimation approaches.

6. REFERENCES

- [1] Oswald M., Stabroth S., Wiedemann C., Wegener P., Martin C., Klinkrad H. "Upgrade of the MASTER Model", Final Report ESA contract 18014/03/D/HK(SC), 2006
- [2] Martin C., Cheese J., Sanchez Ortiz N., Bunte K, Lips T., Fritsche B. Koppenwallner G. "Debris Risk Assessment and Mitigation analysis (DRAMA) Tool", Final Report ESA Contracto No. 16966/02/D/HK
- [3] Alarcon J.-R. "Development of a Collision Risk Assessment Tool", Final report, ESA contract 14801/00/D/HK, GMV S.A., 2002
- [4] Hoots F., Roehrich R. "Spacetrack Report No.3 – Models for the Propagation of NORAD Element Sets" technical report, office of Astrodynamics, Aerospace Defense Center, Peterson AFB, USA, 1980
- [5] Klinkrad H. "Space Debris – Models and Risk Analysis", ISBN 3-540-25448-X, Springer Praxis Publishing Ltd, Chichester, UK, 2006
- [6] Alfriend K., Akella M., Lee D., Frisbee J., Foster J. "Probability of Collision Error Analysis" Space Debris, no.1:21-35, 1999